The Astronomical Journal, 133:906–916, 2007 March

VERY LARGE ARRAY PLUS PIE TOWN ASTROMETRY OF 46 RADIO STARS

D. A. Boboltz,[1] A. L. Fey,[1] W. K. Puatua,[1] N. Zacharias,[1] M. J. Claussen,[2] K. J. Johnston,[1] and R. A. Gaume[1]

Received 2006 June 27; accepted 2006 October 11

ABSTRACT

We have used the Very Large Array, linked with the Pie Town Very Long Baseline Array antenna, to determine astrometric positions of 46 radio stars in the International Celestial Reference Frame (ICRF). Positions were obtained in the ICRF directly through phase referencing of the stars to nearby ICRF quasars whose positions are accurate at the 0.25 mas level. Radio star positions are estimated to be accurate at the 10 mas level, with position errors approaching a few milliarcseconds for some of the stars observed. Our measured positions were combined with previous measurements taken from as early as 1978 to obtain proper-motion estimates for all 46 stars with average uncertainties of $\approx$1.7 mas yr^{-1}. We compared our radio star positions and proper motions with the *Hipparcos* Catalogue data and found consistency in the reference frames produced by each data set on the 1 σ level, with errors of $\sim$2.7 mas per axis for the reference frame orientation angles at our mean epoch of 2003.78. No significant spin is found between our radio data frame and the *Hipparcos* Celestial Reference Frame, with the largest rotation rates of +0.55 and $-$0.41 mas yr^{-1} around the *x*- and *z*-axes, respectively, with 1 σ errors of 0.36 mas yr^{-1}. Thus, our results are consistent with a nonrotating *Hipparcos* frame with respect to the ICRF.

Key words: astrometry — binaries: close — radio continuum: stars — techniques: interferometric

1. INTRODUCTION

The current realization of the International Celestial Reference Frame (ICRF) is defined by the positions of 212 extragalactic objects derived from Very Long Baseline Interferometry (VLBI) observations (Ma et al. 1998; Gambis 1999, p. 87; Fey et al. 2004). This VLBI realization of the ICRF is currently the International Astronomical Union (IAU)–sanctioned fundamental celestial reference frame. At optical wavelengths, the *Hipparcos* Catalogue (Perryman et al. 1997) now serves as the primary realization of the celestial reference frame. The link between the *Hipparcos* Catalogue and the ICRF was accomplished through a variety of ground-based and space-based efforts (Kovalevsky et al. 1997), with the highest weight given to VLBI observations of 12 radio stars by Lestrade et al. (1999). The standard error of the alignment was estimated to be 0.6 mas at epoch 1991.25, with an estimated error in the system rotation of 0.25 mas yr^{-1} per axis (Kovalevsky et al. 1997).

At the epoch of our most recent radio star observations (2004.80) the formal error associated with the *Hipparcos*-ICRF frame link is estimated to be $\sim$3.4 mas. Due to errors in the proper motions, the random position errors of individual *Hipparcos* stars increased from $\sim$1 mas in 1991 to $\sim$12 mas at the time of our most recent observations. Such uncertainties in the frame rotation and the astrometry of individual sources can combine to seriously limit the ability to align high-resolution multiwavelength data on a particular source, thus restricting the astrophysical interpretation of potentially interesting objects.

In this paper we present X-band radio observations of 46 radio stars using the Very Large Array (VLA) in the A configuration linked by fiber optic transmission line to the Very Long Baseline Array (VLBA) antenna located in Pie Town, New Mexico. Both the VLA and VLBA are maintained and operated by the National Radio Astronomy Observatory.[3] The VLA plus Pie Town (VLA+PT) link (Claussen et al. 1999) is a valuable tool for radio star astrometry because it provides the high sensitivity of the VLA with nearly twice the resolution of the VLA A configuration alone for high-declination sources.

The work described herein represents a continuation of a long-term program (since 1978) to obtain accurate astrometric radio positions and proper motions for $\sim$50 radio stars that can be used to connect the current ICRF to future astrometric satellite (e.g., *Gaia* and *Space Interferometry Mission PlanetQuest*) reference frames. These stars were originally selected to be observable at both optical and radio wavelengths, with detectability in the radio being the primary limitation. Quiescent radio flux densities are on the order of 1–10 mJy, with occasional flares of emission >100 mJy. All of the stars have been observed with *Hipparcos* and have spectral types ranging from A to M and visual magnitudes ranging from 0.58 to 10.80. Many of the stars are RS CVn and Algol-type binary systems. Early observations in the program were used to connect the radio frame to the FK4 optical reference frame (Johnston et al. 1985), while later observations were used to link the radio-based ICRF to the *Hipparcos* optical reference frame (Johnston et al. 2003).

The astrometric positions derived from the three epochs of VLA+PT observations are combined with previous VLA (Johnston et al. 1985, 2003), VLA+PT (Boboltz et al. 2003), and Multi-Element Radio Linked Interferometer Network (MERLIN; Fey et al. 2006) positions to determine updated proper motions, $\mu_{\alpha \cos \delta}$ and μ_{δ}, for all 46 sources. Position and proper-motion results obtained for the 46 stars are compared with the corresponding *Hipparcos* values as a measure of the accuracy of our results. Finally, position and proper-motion differences relative to the *Hipparcos* values are computed in order to determine the current (epoch 2004) spin alignment of the *Hipparcos* frame with respect to the ICRF.

2. OBSERVATIONS AND REDUCTION

The VLA+PT radio observations occurred over three epochs: 2003 June 6–7, 2003 September 9–10, and 2004 October 18–19. For the first two epochs, designated experiments AF399a and AF399b, observations occurred over a 24 hr period with 24 and

[1] US Naval Observatory, Washington, DC, USA.
[2] National Radio Astronomy Observatory, Socorro, NM, USA.
[3] The National Radio Astronomy Observatory is a facility of the National Science Foundation operated under cooperative agreement by Associated Universities, Inc.

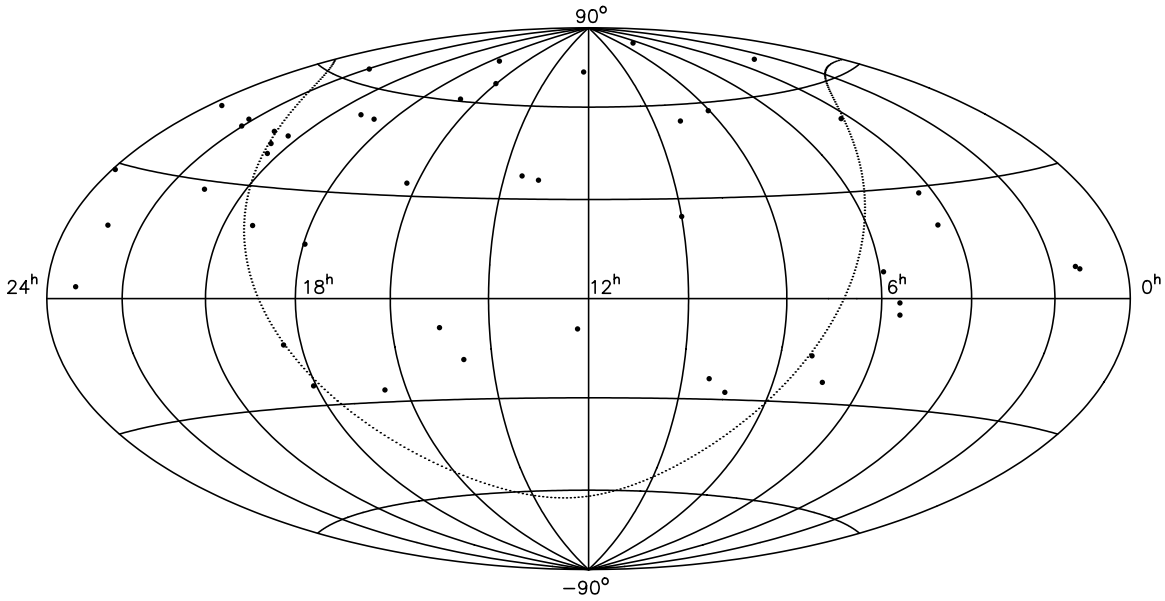

FIG. 1.—Distribution of the 46 observed radio stars plotted on an Aitoff equal-area projection of the celestial sphere. The dotted line represents the Galactic equator.

26 stars observed, respectively. The third epoch was observed over a 10 hr period in which 10 stars not detected in the previous two sessions were reobserved. Data for all three epochs were recorded in dual circular polarization using two adjacent 50 MHz bands centered on rest frequencies of 8460.1 and 8510.1 MHz. The sky distribution of the 46 radio stars detected is shown in Figure 1.

Observations were conducted in a phase-referencing mode by rapidly switching between the star and a nearby ICRF reference source. Listed in Table 1 are the radio star targets along with their associated ICRF calibrators. Also shown in the table are the ICRF positions for each calibrator, the ICRF category, and the separation in degrees between the target and the reference source. Positions for the ICRF reference sources are estimated to be accurate to the 0.25 mas level. For the first two epochs, typical target-calibrator scans lasted 8 minutes with a 2 minute cycle time (90 s on the star and 30 s on the calibrator) for approximately four cycles per scan. For the third epoch the cycle times were increased to 3 minutes (140 s on the star and 40 s on the calibrator) with scans lasting 12 minutes, again resulting in four cycles per scan. Over the course of an experiment, five to eight scans were recorded for each target-calibrator pair over a wide range of hour angles. In addition, periodic scans on the source 3C 48 were performed for the purpose of absolute flux density calibration.

Data were calibrated using the standard routines within the Astronomical Image Processing System (AIPS). The absolute flux density scale was established using the values calculated by AIPS for 3C 48 with the proper *u-v* restrictions applied. Phase calibration was accomplished through transfer of the phases from the reference source to the target source data. From the calibrated data, images were produced for each scan on each target for a total of up to eight images per star per epoch of observations. Average rms noise levels in the CLEANed images from the individual scans were 0.1, 0.09, and 0.04 mJy beam^{-1} for AF399a, AF399b, and AJ315, respectively. Recall that scan times were increased in experiment AJ315 to increase the probability of detecting previously undetected stars from AF399a and AF399b. In addition, a summed image of each star was produced that included data from all scans on the source. Two-dimensional (2-D) Gaussian functions were fit to the emission in the images using the AIPS task JMFIT. For the three experiments, detection rates were 19 out of 24 stars (79%) in AF399a, 21 out of 26 (81%) in AF399b, and 7 out of 11 (64%) in AJ315. For comparison, the detection rate for our VLA+PT radio star pilot study (Boboltz et al. 2003) was 19 out of 19 stars (100%); however, there we purposely tried to select radio stars with high flux densities based on previous observations.

3. RESULTS AND DISCUSSION

3.1. *Source Positions*

Final estimation of source positions and uncertainties was performed outside of AIPS using the results of the 2-D Gaussian fits to the images produced from the observations. Table 2 lists the source positions and associated uncertainties determined for the 46 stars detected over the three epochs. Note that the star HD 193793 appears twice, since it was observed in two experiments, AF399a and AJ315. Because the radio stars were directly referenced to ICRF quasar calibrators using the phase-referencing technique, the positions listed in Table 2 are given directly in the ICRF. Also denoted in the last two columns of Table 2 are the epoch of observation and the number of successful/total observations (scans), which were used in the estimation of position uncertainties for each source. Final positions reported in Table 2 are simply the JMFIT least-squares position estimates from the summed image of each star. The 1 σ position uncertainties listed in the table were estimated using a procedure similar to that described in Fey et al. (2006) and summarized below, depending on whether the source was detected in one or more individual scans.

If a given star was detected in more than one scan, then an rms scatter in the JMFIT scan-based positions weighted by the JMFIT formal errors was computed. The uncertainty in the position reported for each star is then the root sum square (rss) of this weighted rms (wrms) position scatter and the value of the JMFIT least-squares formal uncertainty from the fit to the summed image of the source. The addition of the wrms position scatter was meant to conservatively account for possible systematic errors introduced into the positions by factors such as the variable troposphere. The position uncertainties listed in Table 2 represent the resulting rss values for sources detected in more than one observation.

TABLE 1
OBSERVED RADIO STARS AND CORRESPONDING ICRF CALIBRATOR SOURCES

Star Name	*Hipparcos* Number	ICRF Calibrator	ICRF Category[a]	α (J2000.0)[b]	δ (J2000.0)[b]	Separation (deg)
UV Psc	5980	0119+041	C	01 21 56.861699	04 22 24.73436	2.7
HD 8357	6454	0119+041	C	01 21 56.861699	04 22 24.73436	3.1
RZ Cas	13133	0224+671	D	02 28 50.051459	67 21 03.02926	2.9
B Per	20070	0355+508	O	03 59 29.747262	50 57 50.16151	3.0
HD 283572	20388	0430+289	N	04 33 37.829860	29 05 55.47701	2.7
T Tau N	20390	0409+229	N	04 12 43.666851	23 05 05.45299	4.2
HD 37017	26233	0539−057	D	05 41 38.083384	−05 41 49.42839	2.0
ϵ Ori	26311	0539−057	D	05 41 38.083384	−05 41 49.42839	4.7
α Ori	27989	0529+075	C	05 32 38.998531	07 32 43.34586	5.6
SV Cam	32015	0615+820	D	06 26 03.006188	82 02 25.56764	0.6
HD 50896	33165	0646−306	C	06 48 14.096441	−30 44 19.65940	6.9
R CMa	35487	0727−115	O	07 30 19.112472	−11 41 12.60048	5.4
54 Cam	39348	0749+540	D	07 53 01.384573	53 52 59.63716	3.7
TY Pyx	44164	0919−260	O	09 21 29.353874	−26 18 43.38604	5.1
XY UMa	44998	0850+581	D	08 54 41.996385	57 57 29.93928	4.1
IL Hya	46159	0919−260	O	09 21 29.353874	−26 18 43.38604	2.6
DH Leo	49018	0953+254	O	09 56 49.875361	25 15 16.04977	1.0
HU Vir	59600	1145−071	C	11 47 51.554036	−07 24 41.14109	6.5
DK Dra	59796	1053+704	C	10 56 53.617492	70 11 45.91585	6.7
RS CVn	64293	1315+346	C	13 17 36.494189	34 25 15.93266	2.1
HR 5110	66257	1315+346	C	13 17 36.494189	34 25 15.93266	4.4
RV Lib	71380	1430−178	C	14 32 57.690643	−18 01 35.24885	0.7
δ Lib	73473	1511−100	C	15 13 44.893444	−10 12 00.26435	3.6
AG Dra	78512	1642+690	D	16 42 07.848514	68 56 39.75640	4.4
σ^2 CrB	79607	1611+343	C	16 13 41.064249	34 12 47.90909	0.4
α Sco	80763	1622−253	O	16 25 46.891639	−25 27 38.32688	1.3
WW Dra	81519	1637+574	D	16 38 13.456293	57 20 23.97918	3.4
29 Dra	85852	1749+701	D	17 48 32.840231	70 05 50.76882	4.3
Z Her	87965	1743+173	D	17 45 35.208181	17 20 01.42341	3.7
9 Sgr	88469	1817−254	C	18 20 57.848685	−25 28 12.58456	4.0
FR Sct	90115	1817−254	C	18 20 57.848685	−25 28 12.58456	12.8
BY Dra	91009	1823+568	D	18 24 07.068372	56 51 01.49088	5.3
HR 7275	94013	1954+513	D	19 55 42.738273	51 31 48.54623	7.3
U Sge	94910	1923+210	C	19 25 59.605370	21 06 26.16218	2.3
V444 Cyg	100214	2005+403	O	20 07 44.944851	40 29 48.60414	2.9
HD 193793	100287	2005+403	O	20 07 44.944851	40 29 48.60414	4.1
V729 Cyg	101341	2005+403	O	20 07 44.944851	40 29 48.60414	4.7
HD 199178	103144	2037+511	D	20 38 37.034755	51 19 12.66269	7.4
ER Vul	103833	2113+293	D	21 15 29.413455	29 33 38.36694	3.4
VV Cep	108317	2229+695	D	22 30 36.469725	69 46 28.07698	7.0
RT Lac	108728	2200+420	O	22 02 43.291377	42 16 39.97994	1.6
AR Lac	109303	2200+420	O	22 02 43.291377	42 16 39.97994	3.6
IM Peg	112997	2251+158	O	22 53 57.747932	16 08 53.56089	0.7
SZ Psc	114639	2318+049	C	23 20 44.856598	05 13 49.95266	3.1
λ And	116584	2351+456	O	23 54 21.680266	45 53 04.23653	3.0
HD 224085	117915	2337+264	O	23 40 29.029462	26 41 56.80485	3.8

[a] ICRF source category (Ma et al. 1998; Gambis 1999, p. 87; Fey et al. 2004): D, defining; C, candidate; O, other; N, new in ICRF extension 1.
[b] ICRF extension 1 source positions (Gambis 1999, p. 87). Units of right ascension are hours, minutes, and seconds, and units of declination are degrees, arcminutes, and arcseconds.

If the source was detected in only a single scan, then the reported position uncertainties in Table 2 were estimated by taking the rss of the JMFIT formal position error from the summed image and the average value of the wrms position scatter for all sources with multiple observations in the particular epoch in which the star was observed. There were only three such sources, UV Psc (HIP 5980), SV Cam (HIP 32015), and HR 7275 (HIP 94013), in which the average scatter had to be used, one source in each experiment. For the three experiments, AF399a, AF399b, and AJ315, the average wrms values of position scatter for stars detected in more than one observation were 7.3, 12.1, and 6.3 mas in $\alpha \cos \delta$ and 9.4, 11.1, and 9.9 mas in δ, respectively. Again, this rss step was meant to conservatively account for possible systematic errors in the measured positions.

Table 3 compares the uncertainties in our VLA+PT positions with the corresponding *Hipparcos* uncertainties and lists the rss combined uncertainties for each star. The *Hipparcos* uncertainties have been updated to the epoch of our observations using the reported *Hipparcos* proper-motion errors. Our errors compare favorably with the *Hipparcos* position errors updated to our epoch. The average and median position uncertainties for all 46 stars detected in the VLA+PT observations are 10.2 and 9.2 mas, respectively, in $\alpha \cos \delta$ and 11.5 and 11.3 mas, respectively, in δ. The average and median *Hipparcos* position uncertainties are slightly

TABLE 2
RADIO STAR POSITIONS ESTIMATED FROM THE VLA+PT DATA

Star Name	*Hipparcos* Number	α (J2000.0)[a]	δ (J2000.0)	Epoch	N_{obs}[b]
UV Psc	5980	01 16 55.1402 ± 0.0012 (± 0.018)	06 48 42.242 ± 0.020	2003.6933	1/5
HD 8357	6454	01 22 56.7799 ± 0.0003 (± 0.004)	07 25 10.126 ± 0.006	2003.4356	6/6
RZ Cas	13133	02 48 55.5126 ± 0.0015 (± 0.008)	69 38 03.563 ± 0.010	2003.4356	5/6
B Per	20070	04 18 14.6323 ± 0.0005 (± 0.005)	50 17 43.617 ± 0.004	2003.4356	6/7
HD 283572	20388	04 21 58.8519 ± 0.0015 (± 0.019)	28 18 06.379 ± 0.019	2003.6933	3/5
T Tau N	20390	04 21 59.4364 ± 0.0007 (± 0.009)	19 32 06.394 ± 0.011	2003.6933	5/5
HD 37017	26233	05 35 21.8672 ± 0.0006 (± 0.009)	−04 29 39.013 ± 0.009	2003.6933	6/7
ϵ Ori	26311	05 36 12.8130 ± 0.0005 (± 0.007)	−01 12 06.924 ± 0.012	2003.4356	6/7
α Ori	27989	05 55 10.3097 ± 0.0004 (± 0.005)	07 24 25.461 ± 0.012	2003.4356	7/7
SV Cam	32015	06 41 19.1451 ± 0.0061 (± 0.012)	82 16 01.905 ± 0.012	2003.4356	1/7
HD 50896	33165	06 54 13.0405 ± 0.0023 (± 0.032)	−23 55 42.023 ± 0.025	2003.6933	3/6
R CMa	35487	07 19 28.2380 ± 0.0003 (± 0.004)	−16 23 43.564 ± 0.007	2004.8000	3/5
54 Cam	39348	08 02 35.7663 ± 0.0004 (± 0.003)	57 16 24.834 ± 0.007	2003.6933	5/6
TY Pyx	44164	08 59 42.7071 ± 0.0008 (± 0.011)	−27 48 58.911 ± 0.012	2004.8000	3/5
XY UMa	44998	09 09 55.9135 ± 0.0029 (± 0.025)	54 29 17.044 ± 0.019	2003.6933	3/6
IL Hya	46159	09 24 49.0001 ± 0.0006 (± 0.008)	−23 49 34.859 ± 0.023	2004.8000	5/6
DH Leo	49018	10 00 01.6464 ± 0.0008 (± 0.011)	24 33 09.822 ± 0.014	2003.6933	3/5
HU Vir	59600	12 13 20.6889 ± 0.0007 (± 0.010)	−09 04 46.862 ± 0.016	2004.8000	4/6
DK Dra	59796	12 15 41.4825 ± 0.0032 (± 0.014)	72 33 04.221 ± 0.009	2003.6933	5/6
RS CVn	64293	13 10 36.8927 ± 0.0005 (± 0.006)	35 56 05.658 ± 0.005	2003.4356	7/8
HR 5110	66257	13 34 47.8330 ± 0.0006 (± 0.007)	37 10 56.655 ± 0.003	2003.6933	4/5
RV Lib	71380	14 35 48.4130 ± 0.0005 (± 0.008)	−18 02 11.598 ± 0.011	2003.4356	5/5
δ Lib	73473	15 00 58.3328 ± 0.0005 (± 0.007)	−08 31 08.248 ± 0.011	2003.6933	3/6
AG Dra	78512	16 01 41.0080 ± 0.0030 (± 0.018)	66 48 10.110 ± 0.021	2003.4356	7/8
σ^2 CrB	79607	16 14 40.7704 ± 0.0007 (± 0.009)	33 51 30.688 ± 0.005	2003.6933	4/4
α Sco	80763	16 29 24.4568 ± 0.0005 (± 0.007)	−26 25 55.286 ± 0.014	2003.4356	5/5
WW Dra	81519	16 39 03.9889 ± 0.0014 (± 0.010)	60 41 58.551 ± 0.013	2003.6933	6/7
29 Dra	85852	17 32 41.1473 ± 0.0033 (± 0.013)	74 13 38.567 ± 0.015	2003.6933	7/7
Z Her	87965	17 58 06.9733 ± 0.0009 (± 0.013)	15 08 22.179 ± 0.013	2003.4356	6/6
9 Sgr	88469	18 03 52.4445 ± 0.0009 (± 0.012)	−24 21 38.651 ± 0.022	2003.6933	4/5
FR Sct	90115	18 23 22.7919 ± 0.0008 (± 0.011)	−12 40 51.833 ± 0.017	2003.4356	3/5
BY Dra	91009	18 33 55.8399 ± 0.0013 (± 0.012)	51 43 07.724 ± 0.014	2003.6933	7/7
HR 7275	94013	19 08 25.7296 ± 0.0016 (± 0.014)	52 25 32.351 ± 0.016	2004.8000	1/6
U Sge	94910	19 18 48.4085 ± 0.0002 (± 0.003)	19 36 37.724 ± 0.004	2003.4356	6/6
V444 Cyg	100214	20 19 32.4209 ± 0.0010 (± 0.011)	38 43 53.954 ± 0.008	2003.6933	4/6
HD 193793[c]	100287	20 20 27.9752 ± 0.0004 (± 0.004)	43 51 16.271 ± 0.002	2003.4356	5/6
HD 193793	100287	20 20 27.9747 ± 0.0004 (± 0.004)	43 51 16.268 ± 0.003	2004.8000	4/4
V729 Cyg	101341	20 32 22.4221 ± 0.0008 (± 0.009)	41 18 18.919 ± 0.011	2003.6933	5/5
HD 199178	103144	20 53 53.6634 ± 0.0014 (± 0.015)	44 23 11.089 ± 0.009	2003.4356	6/6
ER Vul	103833	21 02 25.9309 ± 0.0013 (± 0.018)	27 48 26.485 ± 0.017	2003.6933	6/6
VV Cep	108317	21 56 39.1425 ± 0.0019 (± 0.013)	63 37 31.997 ± 0.011	2003.4356	7/7
RT Lac	108728	22 01 30.7601 ± 0.0019 (± 0.021)	43 53 25.734 ± 0.012	2003.6933	7/7
AR Lac	109303	22 08 40.8027 ± 0.0003 (± 0.003)	45 44 32.281 ± 0.004	2003.4356	8/8
IM Peg	112997	22 53 02.2589 ± 0.0002 (± 0.003)	16 50 28.168 ± 0.003	2004.8000	6/6
SZ Psc	114639	23 13 23.7901 ± 0.0001 (± 0.001)	02 40 31.689 ± 0.004	2003.4356	6/6
λ And	116584	23 37 33.8999 ± 0.0009 (± 0.010)	46 27 27.808 ± 0.007	2003.6933	6/6
HD 224085	117915	23 55 04.2039 ± 0.0004 (± 0.005)	28 38 01.356 ± 0.018	2003.4356	7/7

NOTE.—Units of right ascension are hours, minutes, and seconds, and units of declination are degrees, arcminutes, and arcseconds.
[a] Second error (in parentheses) is in arcseconds.
[b] Number of successful/total observations (scans).
[c] HD 193793 was observed in experiments AF399a and AJ315.

larger in $\alpha \cos \delta$ at 12.0 and 10.3 mas, respectively, and slightly smaller in δ at 10.3 and 8.8 mas, respectively.

Listed in columns (9) and (10) of Table 3 are the offsets between our VLA+PT positions and the *Hipparcos* positions updated to the epoch of our observations. These offsets, $\Delta_{Hipp.-\mathrm{radio}}$, are also shown as a function of right ascension in Figure 2 and as a function of declination in Figure 3. Stars observed in the three different experiments are represented by different symbols. Error bars are the combined uncertainties reported in columns (7) and (8) of Table 3. The unweighted mean offsets between our positions and the updated *Hipparcos* positions are 6.1 mas in $\Delta\alpha \cos \delta$ and 0.7 mas in $\Delta\delta$, with standard deviations (σ) of 18.6 and 25.1 mas in $\Delta\alpha \cos \delta$ and $\Delta\delta$, respectively. Unweighted standard errors of the means (σ_M) are then 2.7 mas in $\Delta\alpha \cos \delta$ and 3.7 mas in $\Delta\delta$. Similarly, the mean offsets between the VLA+PT and *Hipparcos* positions, weighted by the square of the rss combined uncertainties, are 2.3 and −0.7 mas with weighted rms errors of 14.3 and 17.4 mas in $\Delta\alpha \cos \delta$ and $\Delta\delta$, respectively.

The unweighted average and median arc length between our measurements and the *Hipparcos* positions is 24.2 and 15.7 mas, respectively, with a standard deviation of 20.5 mas. There are two stars for which the arc length is greater than 75 mas: DH Leo

TABLE 3
RADIO STAR POSITION UNCERTAINTIES AND OFFSETS FROM *Hipparcos*

STAR NAME (1)	*Hipparcos* NUMBER (2)	RADIO ERRORS (mas) $\alpha\cos\delta$ (3)	RADIO ERRORS (mas) δ (4)	*Hipparcos* ERRORS[a] (mas) $\alpha\cos\delta$ (5)	*Hipparcos* ERRORS[a] (mas) δ (6)	COMBINED ERRORS[b] (mas) $\alpha\cos\delta$ (7)	COMBINED ERRORS[b] (mas) δ (8)	$\Delta_{Hipp.-radio}$ (mas) $\alpha\cos\delta$ (9)	$\Delta_{Hipp.-radio}$ (mas) δ (10)
UV Psc	5980	17.8	20.3	13.9	11.2	22.6	23.2	6.6	−51.4
HD 8357	6454	4.4	5.8	12.0	8.1	12.7	10.0	2.2	7.4
RZ Cas	13133	8.0	10.1	5.0	6.8	9.5	12.2	7.0	−1.3
B Per	20070	5.1	4.4	14.3	11.5	15.2	12.3	25.1	−7.5
HD 283572	20388	18.7	19.5	19.2	13.9	26.8	23.9	−22.8	23.2
T Tau N	20390	10.0	11.0	23.0	19.8	25.0	22.6	35.2	−10.9
HD 37017	26233	9.2	9.4	10.6	6.9	14.0	11.6	3.3	−3.6
ϵ Ori	26311	6.9	12.1	9.8	5.4	12.0	13.3	12.1	10.0
α Ori	27989	5.3	12.0	28.1	17.8	28.5	21.5	26.5	4.3
SV Cam	32015	12.4	12.1	11.6	14.3	16.9	18.7	−5.1	−19.2
HD 50896	33165	32.2	25.4	5.3	8.1	32.6	26.7	35.9	29.8
R CMa	35487	3.6	6.6	9.4	9.6	10.0	11.7	8.3	26.3
54 Cam	39348	2.8	6.7	9.5	7.7	9.9	10.2	−9.2	1.7
TY Pyx	44164	10.6	12.3	6.4	7.5	12.3	14.4	2.8	3.6
XY UMa	44998	25.9	19.1	21.1	14.4	33.5	23.9	34.6	−27.7
IL Hya	46159	8.4	23.2	9.9	7.5	13.0	24.4	34.2	−11.2
DH Leo	49018	11.2	13.6	13.7	10.0	17.7	16.9	−49.5	−95.6
HU Vir	59600	9.7	16.2	13.4	9.8	16.6	18.9	22.4	−20.9
DK Dra	59796	8.5	9.1	6.8	6.2	10.9	11.0	0.0	−12.7
RS CVn	64293	6.1	4.9	10.7	8.8	12.3	10.1	13.7	12.0
HR 5110	66257	6.9	3.0	5.5	4.8	8.8	5.6	5.4	−6.9
RV Lib	71380	7.6	11.3	21.5	17.3	22.8	20.7	4.8	−3.8
δ Lib	73473	8.6	10.7	10.5	9.9	13.6	14.6	−18.5	41.5
AG Dra	78512	17.9	21.0	11.2	13.2	21.2	24.8	11.3	10.3
σ^2 CrB	79607	8.7	4.8	10.5	13.7	13.7	14.5	9.0	−4.6
α Sco	80763	7.2	13.9	24.4	16.4	25.5	21.5	19.6	−3.2
WW Dra	81519	10.0	12.6	18.9	18.9	21.4	22.8	34.2	18.6
29 Dra	85852	13.0	15.2	10.6	11.5	16.8	19.1	−20.3	48.2
Z Her	87965	13.0	13.0	8.4	7.8	15.5	15.1	19.5	−20.7
9 Sgr	88469	12.5	21.6	14.7	8.8	19.3	23.3	7.2	16.7
FR Sct	90115	11.0	17.0	19.8	14.1	22.6	22.0	−23.0	74.1
BY Dra	91009	12.5	13.6	8.7	9.4	15.2	16.6	7.7	3.2
HR 7275	94013	14.5	16.0	6.7	6.4	15.9	17.3	44.4	12.7
U Sge	94910	2.9	3.6	6.6	7.1	7.2	8.0	−5.1	−4.6
V444 Cyg	100214	13.1	8.1	8.4	8.4	15.6	11.7	−6.0	−4.0
HD 193793	100287	3.9	2.6	7.1	6.0	8.1	6.5	−14.3	−4.6
HD 193793	100287	4.1	2.3	7.9	6.7	8.9	7.0	−10.4	−4.9
V729 Cyg	101341	8.7	10.9	33.6	29.5	34.7	31.4	26.4	29.8
HD 199178	103144	14.8	8.8	9.4	7.5	17.5	11.5	−18.7	−8.1
ER Vul	103833	17.6	17.4	7.0	7.0	19.0	18.8	8.1	−12.7
VV Cep	108317	12.8	10.7	7.7	5.6	15.0	12.1	7.5	−3.9
RT Lac	108728	20.8	12.0	10.3	11.0	23.2	16.3	1.1	−11.5
AR Lac	109303	3.0	4.0	5.6	6.5	6.4	7.6	2.0	9.1
IM Peg	112997	3.4	3.3	8.3	7.7	8.9	8.4	−5.6	−1.6
SZ Psc	114639	1.4	4.3	14.9	9.9	15.0	10.8	5.4	−12.8
λ And	116584	9.5	6.5	4.0	6.2	10.3	9.0	−1.2	14.0
HD 224085	117915	4.6	17.6	9.7	6.8	10.7	18.9	13.2	5.9

[a] *Hipparcos* uncertainties updated to the epoch of our observations using the *Hipparcos* proper-motion uncertainties.
[b] Combined uncertainties are the rss of our VLA+PT errors and the corresponding *Hipparcos* errors at epoch.

(HIP 49018) and FR Sct (HIP 90115). For both stars the declination offset is the dominant source of the difference from *Hipparcos*; however, neither source has an unusually large uncertainty in declination, 13.6 mas for DH Leo and 17.0 mas for FR Sct. In addition, neither source has a particularly large proper motion in declination, −31.8 and −2.9 mas yr^{-1} for DH Leo and FR Sct, respectively.

DH Leo is an RS CVn binary, as are many of the radio stars on our list. The system is flagged as a component solution in the *Hipparcos* Double/Multiple Systems Annex (Perryman et al. 1997). The annex lists a tertiary component with a separation of 220 ± 20 mas with respect to DH Leo at a position angle of 46° at epoch 1991.25. DH Leo is also listed in the Fourth Catalog of Interferometric Measurements of Binary Stars (Hartkopf et al. 2001) as multiple system CHARA 145. The catalog lists eight measurements of the component separations made with speckle interferometry from epoch 1989.2271 through 1994.2209. Over this 5 yr period the components moved through angles from 38°

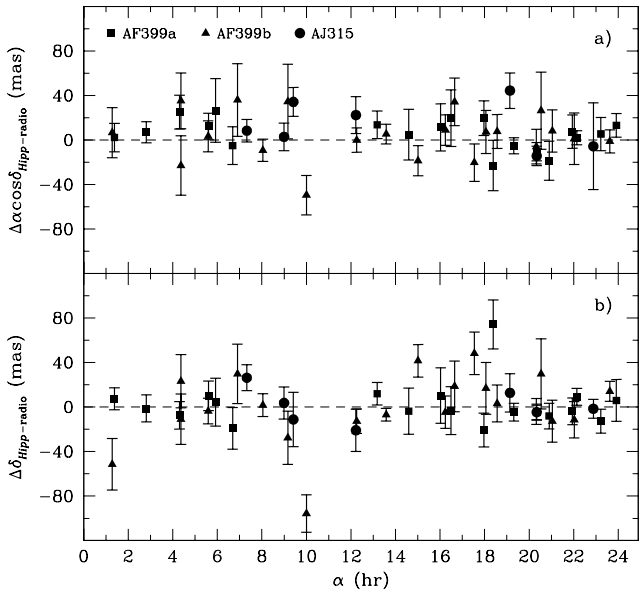

FIG. 2.— Differences between the *Hipparcos* positions updated to the epoch of our observations and our VLA+PT measured positions as a function of source right ascension α for the 46 radio stars observed. Differences in $\alpha \cos \delta$ are plotted in (*a*), and differences in δ are plotted in (*b*). Error bars are the rss combined uncertainties listed in Table 3.

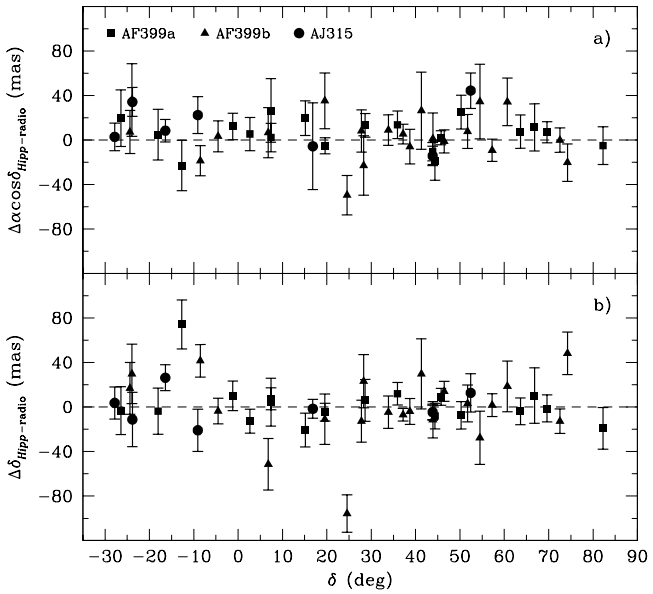

FIG. 3.— Differences between the *Hipparcos* positions updated to the epoch of our observations and our VLA+PT measured positions as a function of source declination δ for the 46 radio stars observed. Differences in $\alpha \cos \delta$ are plotted in (*a*), and differences in δ are plotted in (*b*). Error bars are the rss combined uncertainties listed in Table 3.

to 28° and relative separations of 216–283 mas. It is therefore possible that the 96 mas offset in declination between our radio position and the *Hipparcos* position updated to our epoch is consistent with the orbital motion within the system.

FR Sct, on the other hand, is a single pulsating variable star. The *Hipparcos* Catalogue solution contains no entry in the Double/Multiple Systems Annex (Perryman et al. 1997). In addition, there are no entries for FR Sct in the Washington Double Star Catalog (Mason et al. 2001) or the Fourth Catalog of Interferometric Measurements of Binary Stars (Hartkopf et al. 2001). Therefore, the 74 mas offset in declination between our radio position and the corresponding *Hipparcos* position cannot, as yet, be explained as motion due to a secondary component. It may be that FR Sct is a good candidate for future speckle interferometry observations in light of the offset we have found.

3.2. *Source Proper Motions*

The positions of the 46 radio stars from our VLA+PT observations were combined with previous VLA (Johnston et al. 1985, 2003), VLA+PT (Boboltz et al. 2003), and MERLIN (Fey et al. 2006) positions to determine updated proper motions, $\mu_{\alpha \cos \delta}$ and μ_δ, for all 46 sources. Although the data cover a long time range, 1978–2004, the sampling is not sufficient to enable the determination of source parallaxes. We therefore used the *Hipparcos* values to remove the effects of parallax in our computed proper motions for all 46 stars. Source proper motions were computed using a linear least-squares fit to the data weighted by the position errors for each observation. Position errors for the previous VLA-only observations were estimated to be 30 mas in both $\alpha \cos \delta$ and δ (Johnston et al. 2003), and we have adopted these values. Position errors for previous VLA+PT and MERLIN observations are reported in Boboltz et al. (2003) and Fey et al. (2006), respectively. The proper motions derived from the combined data are listed in Table 4. Also reported are the number of positions used to determine the proper motion ($N_{\rm pos}$) and the total time span between the earliest position measurement and the most recent measurement ($\Delta\tau$). There are three stars, T Tau N (HIP 20390), HD 199178 (HIP 100287), and IM Peg (HIP 112997), for which the time baseline is short, $\Delta\tau < 4$ yr. These three stars are recent additions to our observing list and were not part of the original VLA radio star program (Johnston et al. 1985, 2003).

Table 5 compares the uncertainties in our radio-derived proper motions with the corresponding *Hipparcos* proper-motion uncertainties and lists the rss combined uncertainties for each star. Listed in columns (9) and (10) of Table 5 are the differences between our VLA+PT proper motions and the corresponding *Hipparcos* values. These differences are also shown in Figures 4–8. Figures 4 and 5 show the proper-motion differences $\Delta\mu_{\alpha \cos \delta}$ and $\Delta\mu_\delta$ as a function of right ascension (Fig. 4) and declination (Fig. 5), respectively. The three different symbols represent stars observed in the three corresponding VLA+PT experiments. Error bars are the combined uncertainties reported in columns (7) and (8) of Table 5. Average and median radio-derived uncertainties for the 46 stars are 1.74 and 1.62 mas yr^{-1}, respectively, in $\mu_{\alpha \cos \delta}$ and 1.79 and 1.65 mas yr^{-1}, respectively, in μ_δ. If we exclude the three stars for which $\Delta\tau < 4$ yr, these values drop slightly to 1.59 and 1.62 mas yr^{-1} in $\mu_{\alpha \cos \delta}$ and 1.62 and 1.64 mas yr^{-1} in μ_δ. For comparison, the average *Hipparcos* proper-motion uncertainties are 0.98 and 0.85 mas yr^{-1} in $\mu_{\alpha \cos \delta}$ and 0.84 and 0.72 mas yr^{-1} in μ_δ for the same 46 stars.

The unweighted average differences between our proper motions and the *Hipparcos* values are -0.75 mas yr^{-1} in $\Delta\mu_{\alpha \cos \delta}$ and 0.21 mas yr^{-1} in $\Delta\mu_\delta$, with standard deviations of 2.17 and 2.38 mas yr^{-1} in $\Delta\mu_{\alpha \cos \delta}$ and $\Delta\mu_\delta$, respectively. Unweighted standard errors of the means (σ_M) are thus 0.35 mas yr^{-1} in $\Delta\mu_{\alpha \cos \delta}$ and 0.32 mas yr^{-1} in $\Delta\mu_\delta$. Similarly, the mean offsets between the radio and *Hipparcos* proper motions, weighted by the square of the rss combined uncertainties, are -0.57 and -0.15 mas yr^{-1} with weighted rms errors of 1.77 and 2.26 mas yr^{-1} in $\Delta\mu_{\alpha \cos \delta}$ and $\Delta\mu_\delta$, respectively.

Figures 6, 7, and 8 plot the differences, $\Delta\mu_\delta$ versus $\Delta\mu_{\alpha \cos \delta}$, for the experiments AF399a, AF399b, and AJ315, respectively. Again, the error bars represent the rss combined uncertainties. The figures show that many of the differences between the radio proper motions and those of *Hipparcos* are within the 1 σ error

TABLE 4
Radio Star Proper Motions

Star Name	*Hipparcos* Number	$\mu_{\alpha \cos \delta}$ (mas yr^{-1})	μ_{δ} (mas yr^{-1})	$N_{\rm pos}$[a]	$\Delta\tau$[b] (yr)
UV Psc	5980	84.87 ± 2.36	23.62 ± 2.45	2	14.6893
HD 8357	6454	96.17 ± 1.17	234.07 ± 1.20	3	18.3986
RZ Cas	13133	3.20 ± 1.51	36.55 ± 1.60	5	17.1376
B Per	20070	43.64 ± 1.22	−58.02 ± 1.21	7	21.0065
HD 283572	20388	9.98 ± 1.94	−29.00 ± 1.90	2	18.6563
T Tau N	20390	7.20 ± 4.15	−4.84 ± 5.17	2	2.7484
HD 37017	26233	1.07 ± 1.51	2.63 ± 1.51	4	18.6563
ϵ Ori	26311	−2.12 ± 1.66	−0.91 ± 1.78	3	17.2176
α Ori	27989	23.98 ± 1.04	10.07 ± 1.15	4	21.0175
SV Cam	32015	41.99 ± 1.90	−150.02 ± 1.81	2	17.1376
HD 50896	33165	−3.70 ± 2.06	6.58 ± 1.94	3	20.0172
R CMa	35487	166.19 ± 1.64	−139.38 ± 1.66	2	18.5820
54 Cam	39348	−38.80 ± 1.24	−56.95 ± 1.39	4	21.2672
TY Pyx	44164	−45.68 ± 1.49	−46.24 ± 1.52	3	21.1239
XY UMa	44998	−50.19 ± 2.24	−182.06 ± 2.04	2	17.3953
IL Hya	46159	−42.65 ± 1.98	−30.58 ± 2.39	2	15.7960
DH Leo	49018	−231.88 ± 1.71	−31.78 ± 1.77	2	18.6583
HU Vir	59600	−13.22 ± 1.99	1.33 ± 2.15	2	15.7960
DK Dra	58796	−9.55 ± 1.79	−23.80 ± 1.68	2	18.6583
RS CVn	64293	−50.53 ± 1.39	23.17 ± 1.28	4	21.0145
HR 5110	66257	85.40 ± 1.07	−9.06 ± 0.99	5	21.2752
RV Lib	71380	−20.71 ± 1.79	−18.24 ± 1.86	2	17.2176
δ Lib	73473	−66.16 ± 1.51	−6.19 ± 1.62	6	17.4753
AG Dra	78512	−9.68 ± 2.03	−7.61 ± 2.13	2	17.2176
σ^2 CrB	79607	−267.19 ± 1.31	−86.86 ± 1.22	4	21.2752
α Sco	80763	−10.06 ± 1.07	−23.81 ± 1.24	3	21.0175
WW Dra	81519	22.16 ± 1.26	−60.40 ± 1.32	3	20.0172
29 Dra	85852	−66.85 ± 1.89	33.88 ± 1.92	2	17.4753
Z Her	87965	−26.82 ± 1.67	77.48 ± 1.65	2	19.7596
9 Sgr	88469	0.48 ± 1.62	−3.94 ± 1.85	2	20.0642
FR Sct	90115	0.00 ± 1.66	−2.88 ± 1.74	2	19.8065
BY Dra	91009	186.49 ± 1.60	−325.12 ± 1.65	2	20.0172
HR 7275	94013	−102.73 ± 1.81	−55.05 ± 1.83	2	18.5820
U Sge	94910	0.62 ± 1.62	2.50 ± 1.64	2	18.3986
V444 Cyg	100214	−5.67 ± 1.22	−7.62 ± 1.13	3	20.0172
HD 193793	100287	−4.72 ± 0.66	−1.89 ± 0.64	9	22.3819
V729 Cyg	101341	−2.79 ± 1.44	−5.35 ± 1.48	4	20.0642
HD 199178	103144	27.12 ± 6.14	−1.03 ± 3.51	3	2.4907
ER Vul	103833	89.78 ± 2.39	5.24 ± 2.35	2	14.6893
VV Cep	108317	−4.95 ± 1.64	−2.27 ± 1.61	2	19.8065
RT Lac	108728	57.54 ± 1.72	20.69 ± 1.52	2	21.2672
AR Lac	109303	−52.43 ± 1.02	46.77 ± 1.07	7	21.0095
IM Peg	112997	−18.62 ± 1.34	−27.76 ± 4.22	2	3.8551
SZ Psc	114639	18.64 ± 1.41	27.60 ± 1.43	3	19.8065
λ And	116584	158.77 ± 1.47	−423.50 ± 1.45	2	21.2752
HD 224085	117915	576.20 ± 1.45	34.27 ± 1.67	2	21.0095

[a] Number of position measurements used in the weighted least-squares fit to estimate the proper motion.
[b] Time in years between first and last position epochs.

bars, with the most obvious exception being the star T Tau N in Figure 7. As mentioned previously, T Tau N is one of the stars for which the time baseline is short at only 2.75 yr. In addition, T Tau N is known to be gravitationally bound to the T Tau S binary system with a detected acceleration in its motion (Johnston et al. 2004). With only two positions for T Tau N covering such a short time period it is impossible to fit for any accelerations in the motion of the source with our data alone.

The two stars mentioned previously as having large declination differences relative to *Hipparcos*, FR Sct and DH Leo, appear in Figures 6 and 7, respectively. Although the proper motions in declination (see Table 4) are not very large, the proper-motion differences in declination relative to *Hipparcos* are fairly large at −3.35 mas yr^{-1} for FR Sct and 4.33 mas yr^{-1} for DH Leo. Table 4 shows that both stars have only two position measurements separated by long time intervals between epochs. It is possible that the two stars have an acceleration component in declination that is as yet undetected in the linear fits to our limited data.

3.3. *Radio/Optical Frame Alignment*

Our radio star observations are on the ICRF, while the data taken from the *Hipparcos* Catalogue are on the *Hipparcos* Celestial Reference Frame (HCRF). The *Hipparcos* positions used here have been updated to the epoch of the individual radio star's mean position using the *Hipparcos* proper motions. Following the formulation of Walter & Sovers (2000), the optical minus radio

TABLE 5
RADIO STAR PROPER-MOTION UNCERTAINTIES AND OFFSETS FROM *Hipparcos*

		RADIO ERRORS (mas)		*Hipparcos* ERRORS (mas)		COMBINED ERRORS[a] (mas)		$\Delta\mu_{Hipp.-radio}$ (mas)	
STAR NAME (1)	*Hipparcos* NUMBER (2)	$\mu_{\alpha\cos\delta}$ (3)	μ_δ (4)	$\mu_{\alpha\cos\delta}$ (5)	μ_δ (6)	$\mu_{\alpha\cos\delta}$ (7)	μ_δ (8)	$\mu_{\alpha\cos\delta}$ (9)	μ_δ (10)
UV Psc	5980	2.36	2.45	1.14	0.92	2.63	2.62	0.03	4.39
HD 8357	6454	1.17	1.20	0.98	0.66	1.53	1.37	1.78	3.34
RZ Cas	13133	1.51	1.60	0.41	0.56	1.56	1.69	0.31	−0.92
B Per	20070	1.22	1.21	1.17	0.94	1.69	1.53	−2.95	−1.59
HD 283572	20388	1.94	1.90	1.57	1.14	2.50	2.22	2.46	−1.55
T Tau N	20390	4.15	5.17	1.88	1.62	4.55	5.42	−8.25	7.64
HD 37017	26233	1.51	1.51	0.86	0.56	1.73	1.61	−1.05	1.69
ϵ Ori	26311	1.66	1.78	0.80	0.44	1.85	1.84	−3.61	0.15
α Ori	27989	1.04	1.15	2.30	1.46	2.52	1.86	−3.35	−0.79
SV Cam	32015	1.90	1.81	0.95	1.17	2.12	2.16	0.41	2.89
HD 50896	33165	2.06	1.94	0.43	0.66	2.10	2.05	0.16	1.83
R CMa	35487	1.64	1.66	0.69	0.71	1.78	1.80	0.82	−2.97
54 Cam	39348	1.24	1.39	0.78	0.63	1.46	1.53	−0.52	2.13
TY Pyx	44164	1.49	1.52	0.47	0.55	1.56	1.62	−1.69	−1.44
XY UMa	44998	2.24	2.04	1.73	1.18	2.83	2.36	−2.11	2.61
IL Hya	46159	1.98	2.39	0.73	0.55	2.11	2.46	−5.14	1.62
DH Leo	49018	1.71	1.77	1.11	0.81	2.04	1.95	2.49	4.33
HU Vir	59600	1.99	2.15	0.99	0.72	2.22	2.27	−1.52	1.76
DK Dra	59796	1.79	1.68	0.56	0.51	1.88	1.75	−0.35	1.31
RS CVn	64293	1.39	1.28	0.88	0.72	1.64	1.47	−1.39	1.68
HR 5110	66257	1.07	0.99	0.45	0.39	1.16	1.06	0.70	0.75
RV Lib	71380	1.79	1.86	1.76	1.42	2.51	2.34	−0.17	0.62
δ Lib	73473	1.51	1.62	0.86	0.81	1.74	1.81	0.04	−2.79
AG Dra	78512	2.03	2.13	0.92	1.08	2.23	2.39	−3.50	−2.14
σ^2 CrB	79607	1.31	1.22	0.86	1.12	1.57	1.66	−0.72	0.02
α Sco	80763	1.07	1.24	2.00	1.34	2.27	1.83	0.10	−0.60
WW Dra	81519	1.26	1.32	1.55	1.55	2.00	2.04	−2.60	−2.03
29 Dra	85852	1.89	1.92	0.87	0.94	2.08	2.14	−0.03	−3.19
Z Her	87965	1.67	1.65	0.69	0.64	1.81	1.77	−3.19	3.23
9 Sgr	88469	1.62	1.85	1.20	0.72	2.02	1.99	−0.16	−2.23
FR Sct	90115	1.66	1.74	1.62	1.15	2.32	2.09	1.76	−3.35
BY Dra	91009	1.60	1.65	0.71	0.77	1.75	1.82	−0.13	−0.23
HR 7275	94013	1.81	1.83	0.49	0.47	1.87	1.89	1.69	−0.78
U Sge	94910	1.62	1.64	0.54	0.58	1.71	1.74	−2.32	−0.10
V444 Cyg	100214	1.22	1.13	0.69	0.69	1.40	1.33	0.91	2.06
HD 193793	100287	0.66	0.64	0.58	0.49	0.88	0.80	−2.00	−4.13
V729 Cyg	101341	1.44	1.48	2.75	2.41	3.10	2.83	0.64	0.48
HD 199178	103144	6.14	3.51	0.77	0.61	6.19	3.57	−2.11	−2.68
ER Vul	103833	2.39	2.35	0.57	0.57	2.45	2.42	0.35	0.12
VV Cep	108317	1.64	1.61	0.63	0.46	1.76	1.68	1.53	−0.86
RT Lac	108728	1.72	1.52	0.84	0.90	1.91	1.77	−4.62	1.55
AR Lac	109303	1.02	1.07	0.46	0.53	1.12	1.20	0.23	−0.46
IM Peg	112997	1.34	4.22	0.61	0.57	1.47	4.26	0.05	−1.11
SZ Psc	114639	1.41	1.43	1.22	0.81	1.87	1.64	2.35	−0.17
λ And	116584	1.47	1.45	0.33	0.51	1.51	1.54	0.53	1.54
HD 224085	117915	1.45	1.67	0.79	0.56	1.65	1.76	−0.45	−2.04

[a] Combined uncertainties are the rss of our radio errors and the corresponding *Hipparcos* errors.

position differences are used to determine the relative reference frame orientation angles ϵ_x, ϵ_y, and ϵ_z around the x-, y-, and z-axes, respectively:

$$(\alpha_{\rm HCRF} - \alpha_{\rm ICRF})\cos\delta = \epsilon_x \sin\delta\cos\alpha + \epsilon_y \sin\delta\sin\alpha - \epsilon_z\cos\delta, \quad (1)$$

$$\delta_{\rm HCRF} - \delta_{\rm ICRF} = -\epsilon_x \sin\alpha + \epsilon_y \cos\alpha. \quad (2)$$

Similar formulae are used to obtain the relative spin difference (ω_x, ω_y, and ω_z) of the reference frames using the proper-motion differences between the *Hipparcos* Catalogue and our data. The combined rss formal errors of the *Hipparcos* and our data are used for weighted least-squares adjustments. The weighted mean epoch of our data is 2003.78, and the results, with the sign conventions from equations (1) and (2), are presented in Table 6. The first two rows of the table list the orientation (mas), spin (mas yr^{-1}), and corresponding formal errors for each axis using all 46 stars observed. The HCRF excludes stars flagged for possible multiplicity in the *Hipparcos* Catalogue. Thirteen out of the 46 radio stars we observed have a multiplicity flag in the *Hipparcos* Catalogue; thus, we have excluded them in the second solution

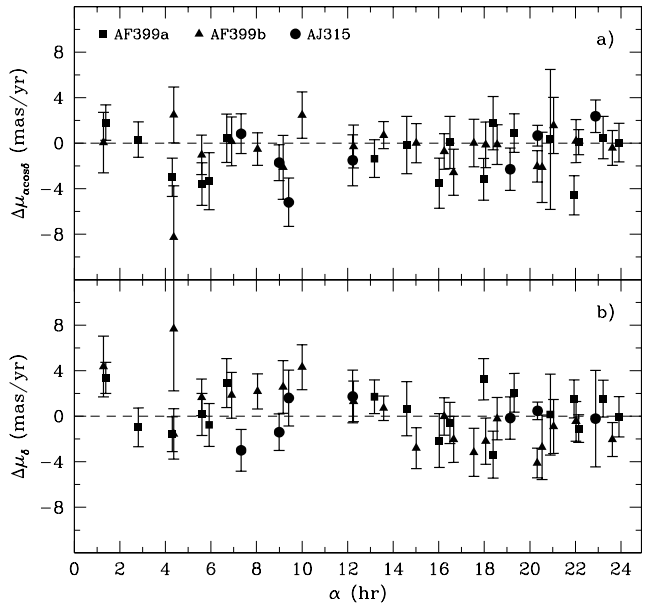

FIG. 4.—Differences between the *Hipparcos* proper motions and our radio-derived proper motions as a function of source right ascension α for the 46 radio stars observed. Differences in $\mu_{\alpha\cos\delta}$ are plotted in (*a*), and differences in μ_δ are plotted in (*b*). Error bars are the rss combined uncertainties listed in Table 5.

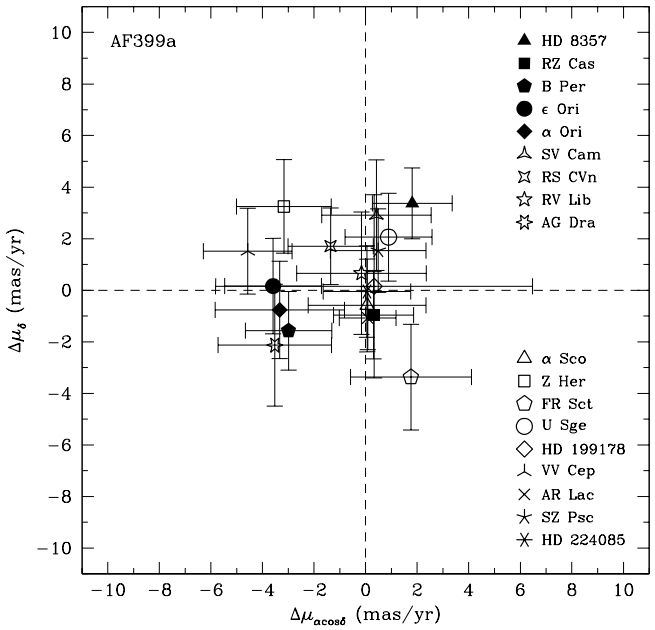

FIG. 6.—Offsets between the *Hipparcos* and radio proper motions, $\Delta\mu_{\alpha\cos\delta}$ vs. $\Delta\mu_\delta$, for the stars observed in VLA+PT experiment AF399a. Error bars are the rss combined uncertainties listed in Table 5.

presented in Table 6 (labeled "33 stars"). Finally, two stars out of the remaining 33 nonmultiple stars showed large postfit residuals in the 33 star rotation solution. These stars are T Tau N, a known multiple, and RZ Cas. A third solution was produced excluding these two stars, and the results are presented in Table 6 (labeled "31 stars").

Because ground-based catalogs often contain systematic errors, especially as a function of declination, preliminary solutions for the orientation angles included an offset in the declination parameter in addition to the three rotation terms. However, these solutions showed the offset term to be insignificant, and the results presented in Table 6 are based on a model including only the three rotation terms. The reduced χ^2 was found to be 1.14 for the position orientation solution and 1.10 for the proper-motion spin solution. This is an indication of small systematic errors, and the addition of an arbitrary rss error of about 5 mas per coordinate per star will bring the χ^2 for the solutions close to 1.0. This additional error was not included in the solutions presented in Table 6.

Updating the *Hipparcos*-ICRF frame alignment discussion presented in Boboltz et al. (2003), the formal, predicted error on the frame alignment at our 2003.78 mean epoch, which is 12.53 yr after the mean *Hipparcos* epoch of 1991.25, is 3.1 mas. The

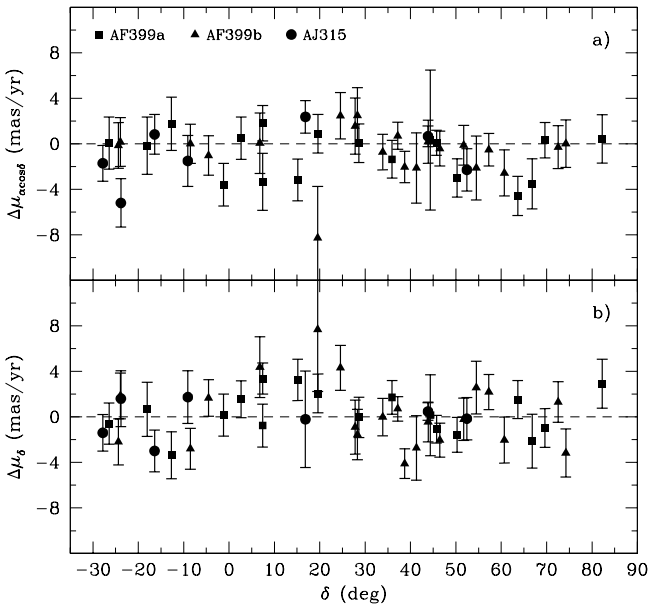

FIG. 5.—Differences between the *Hipparcos* proper motions and our radio-derived proper motions as a function of source declination δ for the 46 radio stars observed. Differences in $\mu_{\alpha\cos\delta}$ are plotted in (*a*), and differences in μ_δ are plotted in (*b*). Error bars are the rss combined uncertainties listed in Table 5.

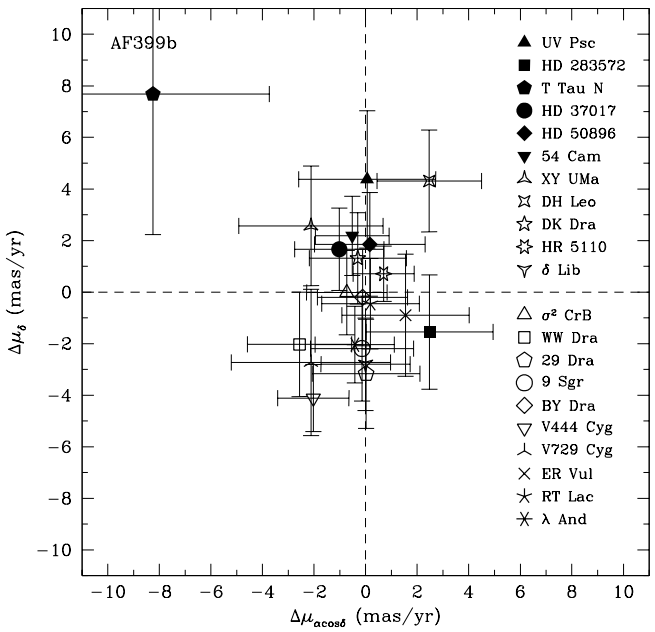

FIG. 7.—Offsets between the *Hipparcos* and radio proper motions, $\Delta\mu_{\alpha\cos\delta}$ vs. $\Delta\mu_\delta$, for the stars observed in VLA+PT experiment AF399b. Error bars are the rss combined uncertainties listed in Table 5.

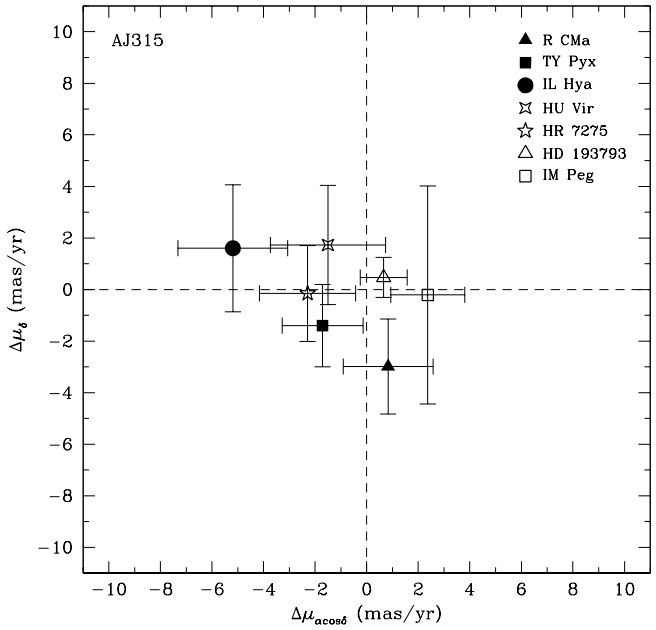

FIG. 8.—Offsets between the *Hipparcos* and radio proper motions, $\Delta\mu_{\alpha\cos\delta}$ vs. $\Delta\mu_\delta$, for the stars observed in VLA+PT experiment AJ315. Error bars are the rss combined uncertainties listed in Table 5.

largest frame orientation angle we find is for the *z*-axis with *Hipparcos* − radio = −3.2 mas, with a formal error of 2.9 mas and thus only a 1 σ (non)significance. The orientations of the *Hipparcos* and ICRF frames are even better for the *x*- and *y*-axes at the 2003.78 mean epoch. For the two alternate solutions with 33 and 31 stars, the frame orientations are slightly larger for the *z*-axis than the 46 star solution and slightly smaller for the *x*- and *y*-axes. All rotation angles are still within the 1 σ formal errors. In addition, the weighted mean offsets between the *Hipparcos* and VLA+PT positions mentioned in § 3.1 (2.3 and −0.7 mas) are consistent with the frame orientation angles and their formal errors.

With the formal errors of the *Hipparcos* data increasing over time and the radio data errors decreasing, it is now appropriate to look, for the first time, at the derivative of the frame orientation, i.e., the proper-motion spin alignment of the frames. We find formal errors in the spin alignment of only about 0.36 mas yr^{-1} per axis for the 46 star solution. This is a factor of 2 improvement over our previous results (Boboltz et al. 2003) and is approaching the original *Hipparcos*-ICRF link error of 0.25 mas yr^{-1}. Our independent observations show the *Hipparcos* frame to be nonrotating with respect to the extragalactic ICRF, with the largest rotation rates being +0.55 and −0.41 mas yr^{-1} around the *x*- and *z*-axes, respectively. These rates are consistent with zero on the 1.6 and 1.1 σ levels, respectively. For the 33 and 31 star solutions, the formal errors are larger at approximately 0.44 mas yr^{-1}. The rotation rate about the *x*-axis was nominally larger with respect to the 46 star solution at $\omega_x \approx 0.62$ mas yr^{-1}, while the rotation rate about the *z*-axis was slightly smaller at $\omega_z \approx -0.31$ mas yr^{-1}. All rotation rates are consistent with zero on a 1.5 σ level or better. The weighted mean proper motion differences mentioned in § 3.2 (−0.57 and −0.15 mas yr^{-1}) are also consistent with these frame rotation rates and their formal errors.

4. CONCLUSIONS

We have determined the astrometric positions for 46 radio stars using the VLA+PT configuration. The positions presented here, with uncertainties on the order of 10 mas or better, are consistent with our earlier VLA+PT results (Boboltz et al. 2003) and represent a factor of 3 improvement over prior VLA-only results (Johnston et al. 1985, 2003). Stellar positions from *Hipparcos* are degrading with time due to errors in the *Hipparcos* proper motions on the order of 1 mas yr^{-1} and due to unmodeled rotations in the frame with respect to the extragalactic objects estimated to be 0.25 mas yr^{-1} per axis. Taking into account these uncertainties, for many of the stars in our list our VLA+PT positions are better than the corresponding *Hipparcos* positions at epoch. The proper motions derived from our VLA+PT positions combined with previous VLA (Johnston et al. 1985, 2003), VLA+PT (Boboltz et al. 2003), and MERLIN (Fey et al. 2006) positions have errors that are on the order of, and in some cases are better than, those obtained from *Hipparcos*.

We have also compared our radio star data with the *Hipparcos* Catalogue data for positions and proper motions and find consistency in the reference frames produced by each data set on the 1 σ level. Errors of ∼2.7 mas per axis were computed for the reference frame orientation angles at our mean epoch of 2003.78 and ∼0.36 mas yr^{-1} per axis for relative spin between the frames. Our independent observations show the *Hipparcos* frame to be nonrotating with respect to the extragalactic ICRF, with the largest rotation rates being +0.55 and −0.41 mas yr^{-1} around the *x*- and *z*-axes, respectively. Future papers will reveal whether this trend has any significance. An independent study based on optical images of extragalactic reference frame sources in combination with dedicated astrograph observations is in preparation (M. I. Zacharias & N. Zacharias 2007). For now, the HCRF orientation and spin are consistent with the ICRF on the 1 σ level of our observations of 46 radio stars.

TABLE 6

Hipparcos MINUS RADIO DATA REFERENCE FRAME ORIENTATION AND SPIN

Solution	ϵ_x (mas)	ϵ_y (mas)	ϵ_z (mas)	ω_x (mas yr^{-1})	ω_y (mas yr^{-1})	ω_z (mas yr^{-1})
All 46 stars	−0.4	0.1	−3.2	0.55	0.02	−0.41
1 σ	2.6	2.6	2.9	0.34	0.36	0.37
33 stars[a]	−1.3	1.2	−2.9	0.61	−0.05	−0.32
1 σ	2.9	2.8	3.2	0.43	0.43	0.46
31 stars[b]	−1.7	0.9	−2.4	0.62	−0.01	−0.30
1 σ	3.1	2.9	3.3	0.43	0.43	0.46

[a] Solution excluding 13 stars with *Hipparcos* multiplicity flags.
[b] Solution excluding 13 *Hipparcos* multiples plus T Tau N and RZ Cas.

REFERENCES

Boboltz, D. A., Fey, A. L., Johnston, K. J., Claussen, M. J., de Vegt, C., Zacharias, N., & Gaume, R. A. 2003, AJ, 126, 484
Claussen, M. J., Beresford, R., Sowinski, K., & Ulvestad, J. S. 1999, BAAS, 31, 1498
Fey, A. L., Boboltz, D. A., Gaume, R. A., Johnston, K. J., Garrington, S. T., & Thomasson, P. 2006, AJ, 131, 1084
Fey, A. L., et al. 2004, AJ, 127, 3587
Gambis, D., ed. 1999, 1998 IERS Annu. Rep. (Paris: Obs. Paris)
Hartkopf, W. I., Mason, B. D., Wycoff, G. L., & McAlister, H. A. 2001, Fourth Catalog of Interferometric Measurements of Binary Stars (Washington: USNO), http://ad.usno.navy.mil/wds/int4.html
Johnston, K. J., de Vegt, C., Florkowski, D. R., & Wade, C. M. 1985, AJ, 90, 2390
Johnston, K. J., de Vegt, C., & Gaume, R. A. 2003, AJ, 125, 3252
Johnston, K. J., Fey, A. L., Gaume, R. A., Claussen, M. J., & Hummel, C. A. 2004, AJ, 128, 822
Kovalevsky, J., et al. 1997, A&A, 323, 620
Lestrade, J.-F., Preston, R. A., Jones, D. L., Phillips, R. B., Rogers, A. E. E., Titus, M. A., Rioja, M. J., & Gabuzda, D. C. 1999, A&A, 344, 1014
Ma, C., et al. 1998, AJ, 116, 516
Mason, B. D., Wycoff, G. L., Hartkopf, W. I., Douglass, G. G., & Worley, C. E. 2001, AJ, 122, 3466
Perryman, M. A. C., et al. 1997, A&A, 323, L49
Walter, H. G., & Sovers, O. J., eds. 2000, Astrometry of Fundamental Catalogues: The Evolution from Optical to Radio Reference Frames (Berlin: Springer)